Structure of spin polarons in the spin-fermion model for CuO_2 planes

Jan Bała
*Max-Planck-Institut für Physik komplexer Systeme, Noethnitzerstrasse 38, D-01187 Dresden, Federal Republic of Germany and Institute of Physics, Jagellonian University, Reymonta 4, PL-30059 Kraków, Poland**

Andrzej M. Oleś
Institute of Physics, Jagellonian University, Reymonta 4, PL-30059 Kraków, Poland
(Received 1 April 1999; revised manuscript received 8 September 1999)

We investigate the spectral functions and various spin-correlation functions relative to the position of the moving oxygen hole in the quantum Néel state formed by copper spins in CuO_2 planes. Solving the problem in a self-consistent Born approximation we have found the spectral functions with the sector of Zhang-Rice states coexisting with higher energy oxygen states, which agree qualitatively with the experimental data in insulating $Sr_2CuO_2Cl_2$. The antiferromagnetic correlations are reduced in the neighborhood of the hole but remain antiferromagnatic and the correlation functions can exhibit similar dipolar distortions as reported in the context of the t-J model. The spectral weight of the quasiparticle decreases as $1/L$ with increasing size of $L \times L$ clusters for the realistic parameters, but remains finite in the thermodynamic limit of CuO_2 planes.

I. INTRODUCTION

The discovery of the high-T_c superconductors[1] started intense theoretical and experimental effort to describe the electronic structure of CuO_2 planes of high-temperature superconducting oxides (HTSO's). It is a generally accepted view that the detailed exploration of their normal phase properties is vital for the explanation of the mechanism of superconductivity in HTSO's. Recent angle-resolved photoemission spectroscopy (ARPES) measurements[2,3] of insulating $Sr_2CuO_2Cl_2$ showed a strongly **k**-dependent low intensity quasiparticle (QP) peak existing only for some momenta at the binding energy near 1 eV. As reported in the recent paper by J. J. M. Pothuizen *et al.*[3] these states can represent Zhang-Rice (ZR) singlets.[4] The singlet character of the lowest energy electron removal states has been shown in the experiment by Tjeng *et al.*[5] These experiments stimulated theoretical investigations of the QP states in the t-J model with extended hoppings,[6–8] and using more realistic Hamiltonians[9–12] describing the motion of a single carrier in a two-dimensional (2D) antiferromagnet.

The t-J model, providing the simplest approximation to the low-energy electronic states of strongly correlated systems gives in presence of antiferromagnetic (AF) correlations the spectral functions with a single QP peak with low dispersion accompanied by a broad featureless incoherent background at higher energies.[13,14] While the t-J model can give only a generic description, the extended t-t'-J (Refs. 6 and 7) and t-t'-t''-J (Ref. 8) models allow to reproduce the dispersion of low-energy QP states in reasonable agreement with the photoemission experiments. The effective parameters t' and t'' may be derived from the multiband tight-binding models using either the cell method[15] or the down-folding procedure.[16] However, these effective one band models are useful only for the low-energy phenomena and are not able to describe the higher energy states observed simultaneously in HTSO's.[17]

To calculate the spectral properties of the entire oxygen-like valence band we consider below a realistic charge-transfer (CT) model which takes into account Cu($3d_{x^2-y^2}$) and all in-plane oxygen orbitals O($2p_\sigma$, $2p_\pi$) playing a dominant role in CuO_2 planes. The π-oxygen states (hybridized with the σ ones) were included as they were also observed with strong momentum dependence at higher energies in the ARPES experiment by Pothuizen *et al.*[3] Integrating out the d^{10} upper and d^8 lower band we derived in previous papers[12,18] an effective model for the planar oxygen states, however, only approximating the umklapp processes by splitting oxygen bands and not including the p_π orbitals. As we show below, the proper treatment of these processes is essential to obtain the spectral functions quantitatively comparable with the results of ARPES experiments.[3] Treating the excitations of the spin system within the linear spin-wave (LSW) theory we calculate the spectral functions in a self-consistent Born approximation (SCBA).[19,20] This approximation proved to be surprisingly accurate for the t-J model,[13,21] and gives also physically expected results for systems with larger spin $S=1$.[22]

Recently Reiter[23] derived a wave function for a single hole in the t-J model to all orders in the number of excited magnons in the AF background which is exact when non-crossing diagrams are included. With the help of the explicit form of the QP wave function corresponding to the SCBA we can gain more information about the character of the hole motion than revealed from the spectral functions. Here, we lean heavily on the work done in the context of the t-J and t-J^z models by Ramšak and Horsch (see Refs. 24 and 25). They made a detailed investigation of various correlation functions around the spin vacancy, finding that all perturbations introduced by a single hole in the quantum antiferromagnet decay at large distances following power laws with dipolar or more complex angular dependencies. Similar studies of the deformation of the spin system for one[26,27] or two holes[28] in the 2D quantum antiferromagnet were performed by exact diagonalization of small clusters.

Whether the QP spectral weight remains finite in the re-

gime referring to underdoped HTSO's approaching the thermodynamic limit is still a controversial issue. There are two different arguments against the QP picture: (i) Anderson[29] argued that the QP weight has to vanish due to the existence of the upper Hubbard band, while (ii) Weng *et al.*[30] claimed that the QP description fails due to the phase-string effect. On the contrary, as shown in the context of the t-J model, a spin-polaron picture can be obtained using a SCBA with nonvanishing QP's (see Ref. 13) in agreement with available results from the finite-size exact diagonalization calculations.[14,26,31]

The paper is organized as follows. In Sec. II we present the effective model for the electronic states in CuO_2 planes. It serves to construct the Reiter wave function for an oxygen hole dressed by spin-wave excitations. The resulting spectral functions and the behavior of different spin-spin correlation functions in the neighborhood of the hole are calculated and discussed in Sec. III. A brief summary and conclusions are presented in Sec. IV.

II. MODEL HAMILTONIAN

The simplest realistic model which describes the holes within the CuO_2 planes of HTSO's is the three-band model with Cu($3d_{x^2-y^2}$) and O($2p_\sigma$) orbitals.[32] However, this model is too oversimplified to describe correctly the experimental photoemission spectrum including the low-lying and higher energy states. Thus we extend it here including O($2p_\pi$) in-plane orbitals. In the limit of weak Cu-O hybridization (t_{pd}) as compared with the Coulomb repulsive energy at copper sites (U) and the CT energy (Δ), i.e., $|t_{pd}| \ll U$ and $|t_{pd}| \ll \Delta$, we derive an effective Hamiltonian, following the procedure described in more detail in Ref. 12.

Treating perturbatively the virtual transitions from the d^9 configurations at Cu sites to higher energy d^8 (low-spin $^1E_1$ states) and d^{10} states, one finds that the electronic states of the CuO_2 plane are described by the following effective spin-fermion model (more details on its derivation from the multiband CT model may be found in Ref. 12):

$$\mathcal{H} = H_s + H_h^0 + H_h^J + H_h^{AF} + H_{h-s}. \tag{2.1}$$

It consists of the superexchange interaction between the Cu spins H_s, the direct oxygen-oxygen hybridization which leads to free hole hopping on the oxygen sublattice H_h^0, the effective oxygen hole hopping terms H_h^J and H_h^{AF}, and the Kondo interactions H_{h-s} between the oxygen holes and copper spins. The latter coupling is responsible for the QP behavior of the oxygen holes at the new energy scale because they cause the dressing of the moving hole by the magnons.[12]

The Kondo interaction

$$H_{h-s} = \sum_{imn} J_K \mathbf{S}_i \cdot \mathbf{s}_{mn} \tag{2.2}$$

describes an effective coupling between the spins of localized holes at copper sites, $\mathbf{S}_i = (S_i^+, S_i^-, S_i^z)$, and the spin density $\mathbf{s}_{mn}$ at the neighboring oxygen sites m and n of the same Cu ion at site i. The oxygen spin operators $\mathbf{s}_{mn}$ are either local ($m=n$) or nonlocal ($m \neq n$),

$$s_{mn}^{+(-)} = a_{m\sigma,\uparrow(\downarrow)}^\dagger a_{n\sigma,\downarrow(\uparrow)},$$

$$s_{mn}^z = \tfrac{1}{2}(a_{m\sigma,\uparrow}^\dagger a_{n\sigma,\uparrow} - a_{m\sigma,\downarrow}^\dagger a_{n\sigma,\downarrow}). \tag{2.3}$$

$a_{m\sigma,\uparrow(\downarrow)}^\dagger$ are hole creation operators in a $2p_\sigma$ orbital at site m. The localized holes occupy the $3d_{x^2-y^2}$ orbitals, and due to the local symmetry only the p_σ orbitals communicate with the Cu($3d$) states. The Kondo interactions in Eq. (2.2) are up to second order,[33]

$$J_K = 2t_{pd}^2 \left(\frac{1}{\Delta_\sigma} + \frac{1}{U - \Delta_\sigma} \right). \tag{2.4}$$

Here we have simplified the notation and write J_K to represent the effective coupling element, whereas in the actual calculations reported in this paper the sign of this element depends on the phases of two different oxygen orbitals, if $m \neq n$ in Eq. (2.2). The first term in the Kondo interaction (2.4) is due to fluctuations to the upper Hubbard band ($d_i^9 p_m^5 \rightleftharpoons d_i^{10} p_m^4$), and the second one involves the transitions to the lower Hubbard band ($d_i^9 p_m^5 \rightleftharpoons d_i^8 p_m^6$). Here Δ_σ is the CT gap for exciting the $3d$ hole on a $2p_\sigma$ orbital of the neighboring oxygen.

In addition to the spin-fermion Kondo interactions, one finds as well the spin-dependent contribution of the form

$$H_h^{AF} = S \sum_{\langle imn \rangle, s} \lambda_s J_K (a_{m\sigma,s}^\dagger a_{n\sigma,s} + \text{H.c.}), \tag{2.5}$$

with $\lambda_s = \pm 1$ for $s = \uparrow, \downarrow$, respectively, and the effective three-site hopping of the oxygen holes,

$$H_h^J = \sum_{\langle imn \rangle, s} T_K (a_{m\sigma,s}^\dagger a_{n\sigma,s} + \text{H.c.}), \tag{2.6}$$

with the effective hopping terms determined by a two-step hopping process via $3d_{x^2-y^2}$ orbitals on the Cu sites,

$$T_K = \frac{1}{2} t_{pd}^2 \left[\frac{1}{\Delta_\sigma} - \frac{1}{U - \Delta_\sigma} \right]. \tag{2.7}$$

As for the Kondo interaction term (2.2), the summations in Eqs. (2.5) and (2.6) labeled by $\langle imn \rangle$ run over the nearest-neighbor oxygen sites m and n of the same Cu ion at site i, and the elements J_K and T_K include the phases of the $3d_{x^2-y^2}$ and $2p_\sigma$ orbitals. For this reason, the three-site hopping couples as well the two oxygen orbitals along the $x(y)$ direction.

The entire hopping part of the effective Hamiltonian, $H_h^0 + H_h^J + H_h^{AF}$, can be diagonalized using the translational symmetry. It is convenient to introduce in the reciprocal space Fourier transforms of the oxygen operators, $a_{\mathbf{k},x(y),\sigma(\pi),s}$, which refer to the basis functions $2p_x$ and $2p_y$, labeled either x or y, and to the type of $2p$ orbital with respect to this particular bond (im), labeled by σ or π,

$$a_{\mathbf{k},x(y),\sigma(\pi)s} = \frac{1}{\sqrt{N}} \sum_{m \in x(y)} a_{m,\sigma(\pi)s} e^{i\mathbf{k}\mathbf{R}_m}, \tag{2.8}$$

where the sum includes a given type $[x(y)]$ of oxygen orbitals. With the help of these operators we rewrite the explicit form of the hole hopping part of the Hamiltonian (2.1) as follows:

$$H_h^0+H_h^J+H_h^{AF}=\sum_{\mathbf{k}\mu\mu' s}[H_h(\mathbf{k})]_{\mu\mu'}a^\dagger_{\mathbf{k}\mu,s}a_{\mathbf{k}\mu',s}, \quad (2.9)$$

where $\mathbf{k}$ is limited to the folded AF Brillouin zone (BZ), and $a_{\mathbf{k}\mu',s}$ represent the following basis states: $a^\dagger_{\mathbf{k},x\sigma s}$, $a^\dagger_{\mathbf{k},y\sigma s}$, $a^\dagger_{\mathbf{k},x\pi s}$, $a^\dagger_{\mathbf{k},y\pi s}$, $a^\dagger_{\mathbf{k}+\mathbf{Q},x\sigma s}$, $a^\dagger_{\mathbf{k}+\mathbf{Q},y\sigma s}$, $a^\dagger_{\mathbf{k}+\mathbf{Q},x\pi s}$, $a^\dagger_{\mathbf{k}+\mathbf{Q},y\pi s}$, for $\mu=1,\ldots,8$, respectively. The explicit form of the 8×8 Hamiltonian matrix $[H_h(\mathbf{k})]_{\mu\mu'}$ is presented in Appendix A.

The spin Hamiltonian H_s is expressed in terms of the Schwinger bosons $b_{i\mathrm{s}}$ (see Refs. 19 and 20) which are expanded around the Néel saddle point: $b_{i\uparrow}=b_{j\downarrow}=0$, $b_{i\downarrow}=b_{j\uparrow}=1$ for $i\in A$ and $j\in B$, where A and B are the sublattices of $\uparrow$ and $\downarrow$ spins in the Néel state, respectively. Performing Fourier,

$$b_{\mathbf{q}}=\frac{1}{\sqrt{N}}\sum_{i\in A}b_{i\uparrow}e^{i\mathbf{q}\cdot\mathbf{R}_i}+\frac{1}{\sqrt{N}}\sum_{j\in B}b_{j\downarrow}e^{i\mathbf{q}\cdot\mathbf{R}_j}, \quad (2.10)$$

and Bogoliubov transformations,

$$\beta_{\mathbf{q}}=u_{\mathbf{q}}b_{\mathbf{q}}-v_{\mathbf{q}}b^\dagger_{-\mathbf{q}},$$
$$u_{\mathbf{q}}=\left[\frac{1+(1-\gamma_{\mathbf{q}}^2)^{1/2}}{2(1-\gamma_{\mathbf{q}}^2)^{1/2}}\right]^{1/2}, \quad (2.11)$$
$$v_{\mathbf{q}}=-\mathrm{sgn}(\gamma_{\mathbf{q}})\left[\frac{1-(1-\gamma_{\mathbf{q}}^2)^{1/2}}{2(1-\gamma_{\mathbf{q}}^2)^{1/2}}\right]^{1/2},$$

with $\gamma_{\mathbf{q}}=1/z\Sigma_\delta e^{i\mathbf{q}\delta}$ (here $z=4$ for a CuO_2 plane), one finds in the LSW approximation the magnon dispersion for a 2D Heisenberg antiferromagnet with $S=1/2$ in the standard form,

$$\omega_{\mathbf{q}}=JzS(1-\gamma_{\mathbf{q}}^2)^{1/2}. \quad (2.12)$$

In the LSW order the total effective Hamiltonian (2.1) represents a coupled hole-magnon problem of the following form:

$$H_{\mathrm{LSW}}=\sum_{\mathbf{k}\mu s}E_\mu(\mathbf{k})p^\dagger_{\mathbf{k},\mu s}p_{\mathbf{k},\mu s}+\sum_{\mathbf{q}}\omega_{\mathbf{q}}\beta^\dagger_{\mathbf{q}}\beta_{\mathbf{q}}$$
$$+\frac{1}{\sqrt{N}}\sum_{\mathbf{kq},\mu\nu s}M_{\mu\nu}(\mathbf{k},\mathbf{q})p^\dagger_{\mathbf{k}-\mathbf{q},\mu s}p_{\mathbf{k},\nu,-s}(\beta^\dagger_{\mathbf{q}}+\beta_{-\mathbf{q}}), \quad (2.13)$$

$E_\mu(\mathbf{k})$ are the eigenvalues of the matrix given by Eq. (2.9) and $p_{\mathbf{k},\mu s}$ are the respective eigenvectors. The vertex $M_{\mu\nu}(\mathbf{k},\mathbf{q})$ has a complex form,

$$M_{\mu\nu}(\mathbf{k},\mathbf{q})=(u_{\mathbf{q}}+v_{\mathbf{q}})\sum_{\xi\xi'=1,2}[F_{\xi\xi'}(\mathbf{k},\mathbf{q})V_{\mu\xi}(\mathbf{k}+\mathbf{q})V_{\nu\xi'}(\mathbf{k})$$
$$+F_{\xi\xi'}(\mathbf{k}+\mathbf{Q},\mathbf{q})V_{\mu\xi}(\mathbf{k}+\mathbf{q}+\mathbf{Q})V_{\nu\xi'}(\mathbf{k}+\mathbf{Q})]. \quad (2.14)$$

This hole-magnon bare vertex depends on the geometrical factors which follow from the Bogoliubov transformations for fermions $\{V_{\xi\mu}(\mathbf{k})\}$ and bosons $\{u_{\mathbf{q}}, v_{\mathbf{q}}\}$. Neglecting the AF corrections to the free Hamiltonian would result in the $M_{\mu\nu}(\mathbf{k},\mathbf{q})$ vertex with the first term in Eq. (2.14) only. The Kondo interaction enters via the coefficients

$$F_{11}(\mathbf{k},\mathbf{q})=J_K\left[\cos\frac{q_x}{2}-\cos\frac{k_x-q_x}{2}\right],$$
$$F_{12}(\mathbf{k},\mathbf{q})=-2J_K\sin\frac{k_x}{2}\sin\frac{k_y-q_y}{2}. \quad (2.15)$$

$F_{22}(\mathbf{k},\mathbf{q})$ and $F_{21}(\mathbf{k},\mathbf{q})$ are obtained from $F_{11}(\mathbf{k},\mathbf{q})$ and $F_{12}(\mathbf{k},\mathbf{q})$, respectively, by the transformation $(k_x,q_x)\leftrightarrow(k_y,q_y)$. The distance Cu-Cu is the unit cell length $a=1$.

Next, we find the Green's function (for $p_{\mathbf{k},\mu\sigma}$ states),

$$G^p_{\mu\nu}(\mathbf{k},\omega)=\frac{1}{\omega-E_\mu(\mathbf{k})\delta_{\mu\nu}-\Sigma^p_{\mu\nu}(\mathbf{k},\omega)}, \quad (2.16)$$

which is determined in the SCBA by the hole self-energy obtained from the bare vertex and the self-consistently dressed Green's function,

$$\Sigma^p_{\mu\nu}(\mathbf{k},\omega)=\frac{1}{N}\sum_{\alpha\beta,\mathbf{q}}M_{\mu\alpha}(\mathbf{k},\mathbf{q})M_{\beta\nu}(\mathbf{k},\mathbf{q})$$
$$\times G^p_{\alpha\beta}(\mathbf{k}-\mathbf{q},\omega-\omega_{\mathbf{q}}). \quad (2.17)$$

We have solved the system of Eqs. (2.16) and (2.17) self-consistently. Next, one has to project the obtained Green's functions on the states with momentum $\mathbf{k}$ only. Consequently, the Green's functions for the *original* $a_{\mathbf{k},x(y),\sigma(\pi),s}$ states have been approximated as

$$G_{ii}(\mathbf{k},\omega)\approx\sum_\nu|V_{i\nu}(\mathbf{k})|^2G^p_{\nu\nu}(\mathbf{k},\omega), \quad (2.18)$$

and the corresponding spectral function for a single hole is given by

$$A_i(\mathbf{k},\omega)=-\frac{1}{\pi}\mathrm{Im}\,G_{ii}(\mathbf{k},\omega+i\epsilon). \quad (2.19)$$

As we show below, the spectral function (2.19) exhibits quite complex structure which, however, resembles the qualitative results obtained for the t-J model.[7,13,31,34]

Knowing the Green's function, we can obtain the Reiter wave function[23,24] which in our model has the following form:

$$|\Psi^{(n)}_{\mathbf{k},i}\rangle=\sqrt{W^{\mathrm{QP}}_{\mathbf{k},i}}\Bigg[p^\dagger_{\mathbf{k},i,s}+\frac{1}{\sqrt{N}}\sum_{\mathbf{q}_1,i_1}M_{ii_1}(\mathbf{k},\mathbf{q}_1)G_{i_1}(\mathbf{k}_1,\omega_1)$$
$$\times p^\dagger_{\mathbf{k}_1,i_1,-s}\beta^\dagger_{\mathbf{q}_1}+\cdots+\frac{1}{\sqrt{N^n}}\sum_{\mathbf{q}_1\ldots\mathbf{q}_n,i_1\ldots i_n}M_{ii_1}$$
$$\times(\mathbf{k},\mathbf{q}_1)G_{i_1}(\mathbf{k}_1,\omega_1)\cdots M_{i_{n-1}i_n}(\mathbf{k}_{n-1},\mathbf{q}_n)$$
$$\times G_{i_n}(\mathbf{k}_n,\omega_n)p^\dagger_{\mathbf{k}_n,i_n,(-1)^n s}\beta^\dagger_{\mathbf{q}_1}\cdots\beta^\dagger_{\mathbf{q}_n}\Bigg]|0\rangle, \quad (2.20)$$

with the momentum, $\mathbf{k}_i=\mathbf{k}-\mathbf{q}_1-\cdots-\mathbf{q}_i$, and energy $\omega_i=\varepsilon_{\mathbf{k}}-\omega_{\mathbf{q}_1}-\cdots-\omega_{\mathbf{q}_i}$ conservation satisfied by each term. The QP energy is determined by $\varepsilon_i(\mathbf{k})=E_i(\mathbf{k})+\Sigma_i[\mathbf{k},\varepsilon_i(\mathbf{k})]$, and $W^{\rm QP}_{\mathbf{k},i}$ stands for the QP spectral weight given by

$$W^{\rm QP}_{\mathbf{k},i}=\frac{1}{1-\dfrac{\partial}{\partial\omega}\Sigma_i(\mathbf{k},\omega)\big|_{\omega=\varepsilon_i(\mathbf{k})}}. \tag{2.21}$$

The QP states are formed mainly by the ''lowest'' oxygen band (lying close to the Fermi energy), and the index i in $|\Psi^{(n)}_{\mathbf{k},i}\rangle$ always refers to this band. The moving hole can not only scatter to a different momentum, but also change its band index. Therefore one finds a more complicated form of the wave function than that known from the t-J model.[24,25] Using the wave function from Eq. (2.20) we have calculated various correlation functions describing the deformation of the AF order in the CuO_2 plane.

III. NUMERICAL RESULTS

A. Parameters of a CuO_2 plane

Below we present numerical results obtained for different values of the CT energies, $\Delta_\sigma=\varepsilon_d-\varepsilon_\sigma$ and $\Delta_\pi=\varepsilon_d-\varepsilon_\pi$, which we used as free parameters in the range $3\leqslant\Delta_{\sigma(\pi)}\leqslant 6$ eV. We have used a similar value of the $p-d$ hopping parameter $t_{pd}=1.4$ eV and of the Coulomb interaction[35] $U=10$ eV to those obtained in the local spin-density approximation for HTSO.[36,37] However, one should be aware of the fact that the estimates of J based on fourth-order term in perturbation theory do not give a reliable value as higher-(fifth) order processes also contribute significantly to the value of this parameter.[38] Therefore the value of $J=0.15$ eV was assumed for the superexchange element; it is close to $J=0.13$ eV which is a generally accepted value in the literature.[38–40] We also included a realistic oxygen dispersion $t_{pp}=0.4$ eV (Ref. 3) and assumed $t'_{pp}=t_{pp}/2$. The model does not include the Cu($3d_{3z^2-r^2}$) and Cu($3d_{xy}$) in-plane orbitals which are rather weakly coupled to oxygen orbitals by the respective hybridization elements and do not contribute significantly to the formation of coherent QP states.[12]

All the numerical calculations were performed on different 2D clusters ranging from 22×22 to 42×42 sites in the $\mathbf{q}$ space with torroidal boundary conditions in the irreducible wedge of the unfolded BZ. The energy axis ω was divided into 500 points per 1 eV and we have stopped iterating when the changes in $\Sigma_{\mathbf{k},\omega,i}A_i(\mathbf{k},\omega)^2$ became less than 0.1–0.01% (this corresponds to 20–40 iterations, depending on the parameters). Except for Fig. 1 very small broadening $\epsilon=0.005$ eV was used. Larger ϵ leads to broadening of the main maxima with no apparent change in the incoherent part of the spectra and the positions of the main maxima.

B. Spectral functions

First, we show that the spectral functions obtained by solving the spin-fermion model within the SCBA are quite different from those found for free oxygen bands, and agree very well with the experimental results for the realistic parameters of the model (2.1). The oxygen spectral functions along the $(0,0)-(\pi,\pi)$ direction (where the strongest ZR states have been observed[2,3]) are displayed in Fig. 1. Without the AF background due to Cu spins the spectral functions would consist of four peaks corresponding to four oxygen bands. The AF order induces a local alternating potential (H_h^{AF}) which acts on the moving oxygen hole, and gives up to *eight* states obtained by diagonalizing the Hamiltonian $H_h^0+H_h^J+H_h^{AF}$ (2.9) [see Fig. 1(a)]. They are characterized by strong $\mathbf{k}$ dependence of the corresponding subbands. At the high-symmetry points (0,0) and (π,π) several of these states become degenerate and one finds only two strong QP peaks for σ and π oxygen states, respectively.

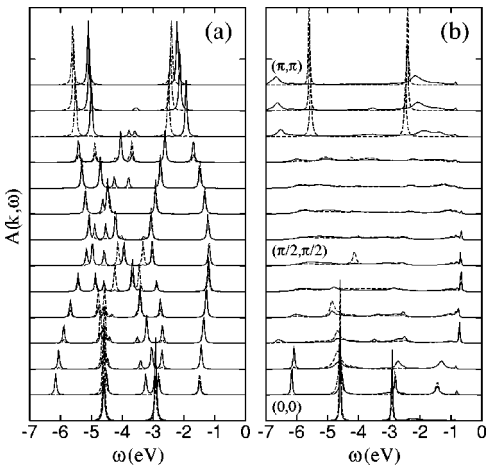

FIG. 1. The electronic spectral functions as obtained for the realistic parameters along the (0,0)-(π,π) direction with $\Delta_\sigma=4.5$ eV, $\Delta_\pi=5.0$ eV: (a) the total free Hamiltonian [see Eq. (2.9)], and (b) including the hole-spin coupling in the Born approximation. Solid and dashed lines stand for states with σ and π symmetry, respectively. The broadening of: (a) $\epsilon=0.03$ eV and (b) $\epsilon=0.015$ eV was used.

Next, in Fig. 1(b) we presented the spectra obtained when the interactions with magnons are included in the SCBA. The QP peaks are drastically modified with respect to those in Fig. 1(a). Close to the $(\pi/2,\pi/2)$ point the formation of the ZR singlets found at $\omega\approx-0.8$ eV [which appear about 0.5 eV above the highest free oxygen band at $\mathbf{k}=(\pi,\pi)$] is accompanied by completely incoherent oxygen states at higher excitation energies (i.e., more distant from the Fermi energy). Approaching the (π,π) point we have found $2p_\pi$ coherent bandlike states at $\omega\approx-2.4$ eV, in agreement with the symmetry considerations (see Fig. 3 of Ref. 3). Moreover, our calculations also predict similar $2p_\pi$ bandlike states at $\omega\approx-5.6$ eV [see Fig. 1(b)] which has not been reported yet. In the σ sector close to the (π,π) point the lower band at $\omega\approx-5$ eV from Fig. 1(a) change into an antibound state at $\omega\simeq-6.5$ eV, while the upper one at $\omega\simeq-2.0$ eV gives a broad incoherent feature due to its dressing by the magnons [compare Fig. 1(a) with Fig. 1(b)].

The intensity of the QP states close to the Fermi energy strongly depends on the momentum $\mathbf{k}$, reflecting the coupling of the moving hole to spin background tuned by the vertex $M_{\mu\nu}(\mathbf{k},\mathbf{q})$ in Eq. (2.13) which is weak in a large part of the BZ.[10] However, except for the (0,0) point where the vertex vanishes, very little of bandlike states survives in the

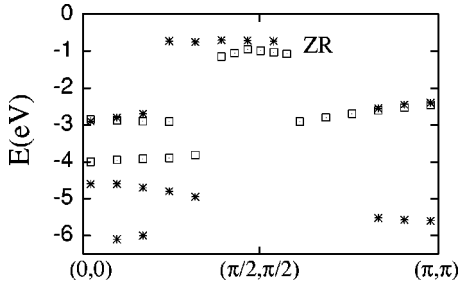

FIG. 2. Positions of the main maxima in the calculated spectra from Fig. 1 (*) and in the ARPES data of Ref. 3 (□) along the (0,0)-(π,π) direction. Low-energy bound (Zhang-Rice) states are indicated by ZR.

σ channel. It is quite remarkable that the coupling between the π and σ channels which is quite weak, is nevertheless able to change the π sector quite considerably. As a result, the higher energy spectrum is completely incoherent at intermediate momenta.

A correct interpretation of the ARPES spectra of the cuprates is an outstanding problem. Early attempts focused on the low-energy part of the spectral function with a state with low dispersion which can be fitted by the *t-J* model.[6,7] This QP state can be even fitted using a mean-field approach within the three-band model for an undoped insulator where the polaronic effects are absent.[41] Here we approach this problem by including both mean-field processes in the effective spin-fermion model, and the polaronic effects which, as we show, change the spectra in a rather dramatic way.

It is very encouraging that the main features seen in the experiment of Pothuizen *et al.*[3] are reproduced by the present model calculation (see Fig. 2), reproducing even the asymmetry of the intensity in the ZR states around the point $(\pi/2,\pi/2)$. Our calculations predict also the QP states close to the $(\pi,0)$ point, where the bound states were also observed by Wells *et al.*[2] As seen in Fig. 1(b), the ZR states are built up of states coming from both sectors (solid and dashed lines). Thus for $t'_{pp}\neq 0$ both p_σ and p_π orbitals are active in the formation of bound states and one may consider instead the oxygen orbitals rotated by $\pi/4$ which replace the ones directed along the *x* or *y* direction. The prominent role of p_π orbitals in the formation of ZR states is also observed in the photoemission experiment of Pothuizen *et al.*,[3] where a strong feature at (π,π), originating from p_π orbitals, has a strong intensity variation with **k**, and disappears close to the $(\pi/2,\pi/2)$ point in the BZ [see Fig. 1(a) in Ref. 3]. Furthermore, close to the (0,0) point we have found two strong QP peaks in the same energy region as measured in $Sr_2CuO_2Cl_2$. Some discrepancies between our spectral functions and the ARPES results may come from the interaction with $3d_{3z^2-r^2}$ or $3d_{xy}$ orbitals, or from out-of-plane oxygen states which are not included in our model.

Finally, we present in Fig. 3 the self-energy, $\Sigma(\mathbf{k},\omega)$, calculated at the QP-band minimum. The QP bound state manifests itself by the minimum in both $\mathrm{Re}\,\Sigma(\mathbf{k},\omega)$ and $\mathrm{Im}\,\Sigma(\mathbf{k},\omega)$ at $\omega\simeq -0.8$ eV. Moreover, one can find strong minimum in $\mathrm{Im}\,\Sigma(\mathbf{k},\omega)$ at $\omega\simeq -4.3$ eV close to the band oxygen states [see Fig. 1(b)]. At intermediate energies $\omega\approx -4$ eV $\mathrm{Re}\,\Sigma(\mathbf{k},\omega)$ changes sign being negative (positive) in the low (high) energy sector. Positive $\mathrm{Re}\,\Sigma(\mathbf{k},\omega)$ at momenta close to the (π,π) point in the high-energy sector is responsible for the formation of unbound states at $\omega\simeq -6.5$ eV. Both parts of the self-energy have similar behavior as found for the *t-J* model calculations (see, e.g., Fig. 8 in Ref. 13), but with weaker oscillations in the bound-state sector.

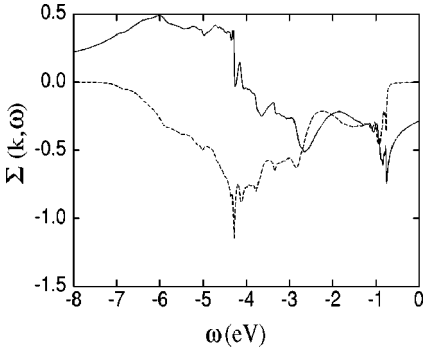

FIG. 3. The hole self-energy $\Sigma(\mathbf{k},\omega)$ (in eV) calculated at the minimum of QP-band found at $\mathbf{k}=(0.45\pi,0.45\pi)$ for the parameters as in Fig. 1. Solid and dashed lines correspond to the real and imaginary parts of the self-energy, respectively.

C. Correlations around an oxygen hole

We turn now to the structure of the wave function for a single hole in the spin-fermion model (2.20), and study the physical consequences of adding a hole in the spin-fermion model by evaluating various spin-correlation functions. Let us first estimate the number of magnons which have to be included in the wave-function $|\Psi^{(n)}_{\mathbf{k},i}\rangle$ in further numerical analysis in order to represent with sufficient accuracy the infinite expansion (2.20) by a finite order.[42] In Fig. 4 we present the norm $\mathcal{N}^{(n)}_{\mathbf{k}}$ (B1) of the wave function $|\Psi^{(n)}_{\mathbf{k},i}\rangle$ as a function of the superexchange element *J*, calculated for different number of magnons included in the wave function, and for the momentum **k** selected at the minimum of the QP band. We have found that already for $J\geqslant 0.15$ eV it is sufficient to include only $n=3$ terms in the wave function in order to reproduce more than $\sim 96\%$ of the norm of the wave function, while the same level of accuracy is obtained with only two magnons for $J>0.3$ eV. In the weak-coupling regime of $J>0.6$ eV one magnon is sufficient, and the QP

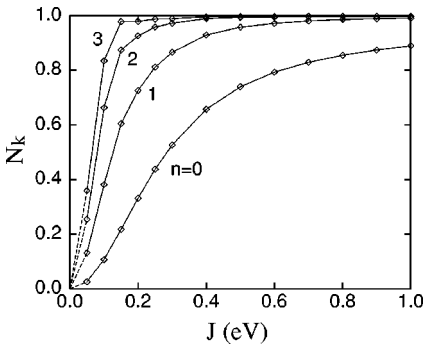

FIG. 4. The norm $\mathcal{N}_{\mathbf{k},i}$ as a function of *J* including magnons up to order $n=3$ in the QP wave function (2.20) for the momentum $\mathbf{k}=(0.45\pi,0.45\pi)$ which corresponds to the minimum of the QP band at $\Delta_\sigma=\Delta_\pi=5.0$ eV.

TABLE I. QP weight ($n=0$) and the norm $\mathcal{N}_{\mathbf{k}}^{(n)}$ ($n=1,\ 2,\ 3$) [given by Eq. (B1)] for the momentum at the minimum of the QP band as a function of the CT energies $\Delta_\sigma=\Delta_\pi$ (in eV). Other parameters as defined in Sec. III.

$\Delta_\sigma=\Delta_\pi$	$n=0$	$n=1$	$n=2$	$n=3$
3.5	0.183	0.510	0.787	0.935
4.0	0.174	0.581	0.864	0.972
5.0	0.376	0.754	0.918	0.962
6.0	0.490	0.822	0.931	0.955

peak due to the $n=0$ component grows steadily with increasing J. In contrast, the strong-coupling regime of small $J<0.15$ eV is characterized by a rapid decrease of $\mathcal{N}_{\mathbf{k}}^{(n)}$ for $n=2$ and 3, and this decrease is much faster that in the t-J model (compare Fig. 4 with Fig. 6 in Ref. 25). This suggests that a moving hole dresses easier by spin excitations in the present spin-fermion model as a result of a strong Kondo coupling J_K.

In general, also increasing CT energy Δ stabilizes the QP states, as shown in Table I. The increase of the spectral weight from 0.174 to 0.490 between $\Delta=4.0$ and 6.0 eV is very strong, while the change in the polaron shape is responsible for a decrease of the QP weight between $\Delta=3.5$ and 4.0 eV. In the range of $3.5<\Delta<6.0$ eV one finds more than 93% of the norm by including $n=3$ magnon excitations. A small decrease of $\mathcal{N}_{\mathbf{k},i}^{(3)}$ from $\Delta=4.0$ to 6.0 eV results from the decrease and change of sign of the effective hopping $\propto T_K$ and from the decrease of J/J_K for $\Delta>5.0$ eV.

Before we address the results obtained for various spin-correlation functions, let us analyze the calculation procedure. The distribution of bosons around the oxygen hole is defined by the correlation function

$$N_{\mathbf{R}}=\langle n_0 b_{i\uparrow(\downarrow)}^{\dagger} b_{i\uparrow(\downarrow)}\rangle, \tag{3.1}$$

where $n_0=(1/N)\Sigma_{\mathbf{k},\mathbf{k}'}\Sigma_{\mu s} p_{\mathbf{k}\mu s}^{\dagger} p_{\mathbf{k}\mu s}$ is the oxygen hole density operator at $R_m=0$, and the average is calculated with respect to the wave function (2.20), $\langle\cdots\rangle=\langle\Psi_{\mathbf{k},i}^{(n)}|\cdots|\Psi_{\mathbf{k},i}^{(n)}\rangle$. The boson number operator $b_{i\sigma}^{\dagger}b_{i\sigma}$ generates qualitatively new vertices $V_1(\mathbf{q_1},\mathbf{q_2})$ and $V_2(\mathbf{q_1},\mathbf{q_2})$, in addition to the hole-magnon vertices which follow from the interaction term (2.13). They describe either scattering of a magnon on a hole, or creation (annihilation) of two magnons (see Fig. 5) and have the same form as those used by Ramšak and Horsch[25] in their calculations for the t-J model,

$$V_1(\mathbf{q_1},\mathbf{q_2})=\tfrac{1}{2}(u_{\mathbf{q}_1}u_{\mathbf{q}_2}+v_{\mathbf{q}_1}v_{\mathbf{q}_2})e^{i(\mathbf{q}_1-\mathbf{q}_2)\mathbf{R}},$$

$$V_2(\mathbf{q_1},\mathbf{q_2})=\tfrac{1}{2}(u_{\mathbf{q}_1}v_{\mathbf{q}_2}+u_{\mathbf{q}_2}v_{\mathbf{q}_1})e^{i(\mathbf{q}_1+\mathbf{q}_2)\mathbf{R}}. \tag{3.2}$$

In Fig. 5 we have presented diagrams which were included in the evaluation of the correlation function $N_{\mathbf{R}_i}$; the corresponding analytic expressions are given in Appendix B. The diagrams were evaluated self-consistently with the dashed lines standing for a self-consistent hole propagator. The numerical computations are much longer than for the one band t-J model for two reasons: (i) the QP peaks are not so well separated from the rest of the spectrum and consequently the energy step $\Delta\omega$ has to be smaller; (ii) the band

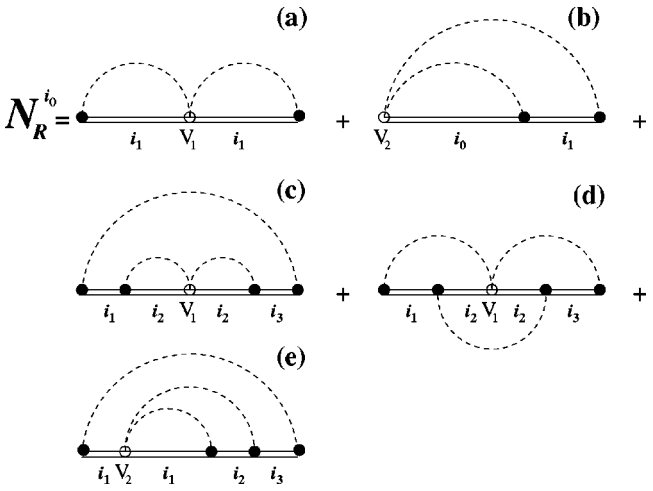

FIG. 5. Diagrams included in the numerical calculations of spin deviations around the hole (and other correlations functions). Two-magnon vertices V_1 and V_2 (3.2) are shown by empty circles, while the one-magnon processes contained in the wave function (2.20) are shown by full circles.

indices $i_1,\ i_2,\ i_3=1,\ldots,8$ make the individual diagrams from Fig. 5 about 8^2 times longer to evaluate than the respective diagrams in the t-J model. For these reasons we had to omit three additional diagrams of order 8^3 [similar to Figs. 5(c) and 5(d) with one more bosonic line] which give, however, smaller contributions than the diagrams shown in Fig. 5.

In Figs. 6 and 7 we display the distribution of bosons around the oxygen hole. As presented in Fig. 6 the spin polaron formed around the hole is extended in the $\langle 11\rangle$ direction of the hole momentum, reflecting the asymmetry of the QP band energy. This asymmetry is similar to that found before for the t-J model.[24] However, in the $\langle 1\bar{1}\rangle$ direction we also found considerable spin fluctuations which were not present for the spin polaron in the t-J model. As a qualitative difference to the t-J model, for smaller CT elements $\Delta_\sigma=\Delta_\pi=4.0$ eV we found a completely different spatial structure of the polaron which extends instead in the $\langle 10\rangle$ and $\langle 01\rangle$ directions (Fig. 7), reflecting the symmetry of the square lattice. Thereby the largest changes are found on one sublattice, indicating that the oxygen hole couples strongly to

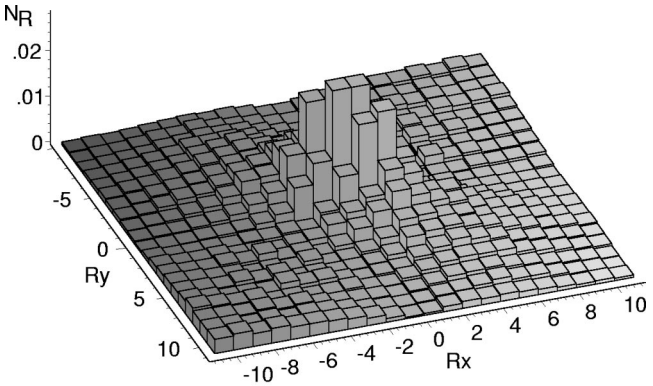

FIG. 6. Distribution of spin deviations around the hole, $N_{\mathbf{R}}$ calculated at the QP-band minimum at $\mathbf{k}=(0.45\pi,0.45\pi)$ for: $\Delta_\sigma=\Delta_\pi=5.0$ eV.

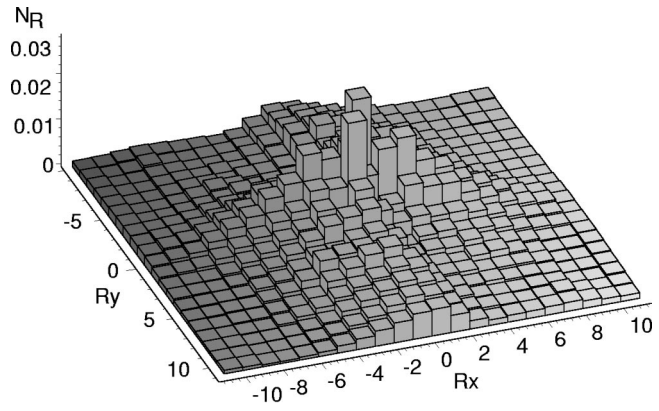

FIG. 7. Distribution of spin deviations around the hole, $N_{\mathbf{R}}$ calculated at the QP-band minimum at $\mathbf{k}=(0.45\pi,0.45\pi)$ for $\Delta_\sigma=\Delta_\pi=4.0$ eV.

the copper sites with the opposite spin direction. A similar shape of the polaron as in Fig. 7 is found for even smaller $3<\Delta_\sigma<4$ eV. Further decrease in the CT elements leads to very weak and less coherent ZR sector, while the second-order procedure used in our model is no longer reliable. On the whole, the spin deviations created by the hole motion are weaker than obtained in the *t-J* model as the spin-fermion approach to the hole motion is by construction in the intermediate-coupling regime while the *t-J*-type model represents the strong-coupling limit of the problem.

The modification of the nearest-neighbor spin-spin correlation function due to the presence of the hole is expressed by

$$C_{\mathbf{R}}=\langle n_0(\mathbf{S}_i\mathbf{S}_j)\rangle, \tag{3.3}$$

where $\mathbf{R}=\frac{1}{2}(\mathbf{R}_i+\mathbf{R}_j)$ labels the bond between two neighboring copper sites i and j. The $C_{\mathbf{R}}$ function was evaluated relative to its background value in the undoped antiferromagnet,

$$C_0=\left[-\frac{1}{4}+\frac{1}{N}\sum_{\mathbf{q}} v_{\mathbf{q}}^2+\frac{1}{N}\sum_{\mathbf{q}} \cos[\mathbf{q}(\mathbf{R}_i-\mathbf{R}_j)]u_{\mathbf{q}}v_{\mathbf{q}}\right]\langle n_0\rangle, \tag{3.4}$$

giving for a 2D square lattice the well-known result $C_0\simeq -0.329\langle n_0\rangle$.[24] The nearest-neighbor spin-correlation function $C_{\mathbf{R}}$ defined on the bonds which connect two nearest copper sites separated by one oxygen ion (3.3) is shown as a function of the superexchange element in Fig. 8. AF correlations persist in the vicinity of the oxygen hole and the ferromagnetic polaron picture is not realized here at $J=0.15$ eV and larger. This shows that due to the extended character of spin polaron, the magnetic correlations in the doped CuO_2 planes are less susceptible to the Kondo interaction element J_K than one might expect from the solution of small clusters in the strong-coupling regime.[33] In agreement with intuition, in both cases of $\Delta_\sigma=\Delta_\pi=5.0$ and 4.0 eV, the strongest deformations of the quantum Néel order are found on the same Cu–Cu bond where the hole is added, being ~ 0.03 and ~ 0.055 at $J=0.15$ eV, respectively [Figs. 8(a) and 8(b)]. We observe the change of local symmetry of the spin-spin corrections from the $\langle 11\rangle$ to $\langle 10\rangle$ direction.

In contrast to the *t-J* model where four bonds around an added hole are *removed*, the oxygen hole can affect only a

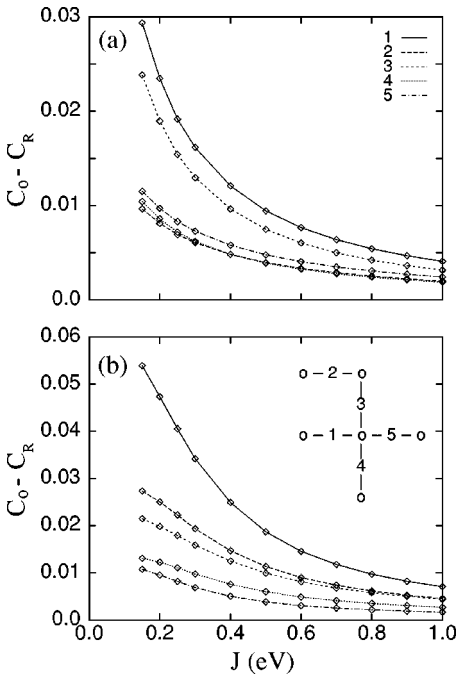

FIG. 8. Nearest-neighbor spin-spin correlation function $C_{\mathbf{R}}$ as a function of the superexchange interaction J calculated at the QP-band minimum at $\mathbf{k}=(0.45\pi,0.45\pi)$ for (a) $\Delta_\sigma=\Delta_\pi=5.0$ eV, and (b) $\Delta_\sigma=\Delta_\pi=4.0$ eV. The inset in (b) shows the labels of Cu–Cu bonds for which the data are shown (○ are the copper sites). The hole is located at oxygen in the center of bond 1.

single Cu-Cu bond at a time, distracting the superexchange processes going through this particular bond. However, the direction of each Cu spin located next to the hole is determined by three other neighboring copper spins, and one cannot thus expect larger changes in $C_{\mathbf{R}}$ than by about 25% of its asymptotic value -0.329. In the *t-J* model the AF correlations are much stronger disturbed by the added hole, as found in the charge and spin distribution functions, $C_{\mathbf{R}}$ and $N_{\mathbf{R}}$, by Ramšak and Horsch.[24,25]

Another interesting information about the deformation of spin background by the added hole is contained in the bond spin currents $\mathbf{j}_{\mathbf{R}}$. As the total spin is not conserved, we consider only the z component of the current operator defined by

$$j_{\mathbf{R}}=\langle n_0(\mathbf{S}_i\times\mathbf{S}_j)u^z\rangle, \tag{3.5}$$

with a unit vector $\mathbf{u}=\mathbf{R}_2-\mathbf{R}_1$. We have studied the currents $j_{\mathbf{R}}$ for the same sets of parameters as above (see Fig. 9). The currents are much weaker than those found by Ramšak and Horsch for the spin polaron in the *t-J* model,[24,25] and vanish on the bond with an oxygen orbital occupied by a hole. A sharp difference in the polaron shape between two different values of CT gaps $\Delta=5.0$ and 4.0 eV, as represented by $N_{\mathbf{R}}$ function (see Figs. 6 and 7), is also reflected in the spin currents on different bonds. If the $\langle 11\rangle$ polarons are formed at $\Delta=5$ eV, the largest currents are found on bonds labeled 3 and 2, while large current on the bond 5 found for $\Delta=4$ eV shows that the backflow of spin is large along the same direction as the direction of the bond which contains the oxygen hole.

Finally, we have addressed the problem of the lattice size dependence of the spectral weight $a_{\mathbf{k}}$ in the QP peak evalu-

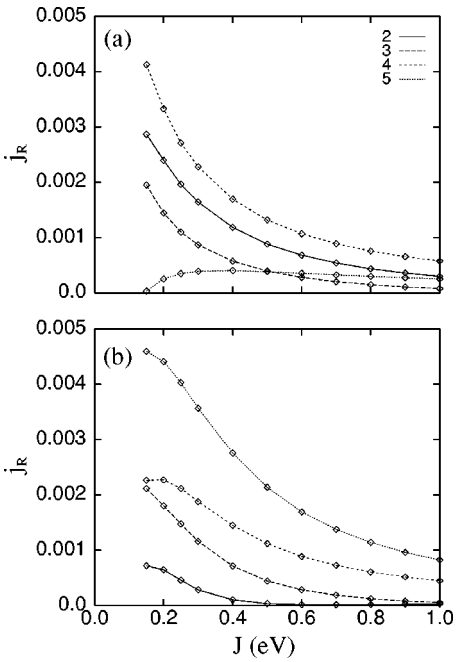

FIG. 9. The z component of the bond spin currents $j_{\mathbf{R}}$ as a function of the superexchange interaction J calculated for the same parameters as in Fig. 8. The labels of Cu–Cu bonds are the same as defined in the inset in Fig. 8(b).

ated at the bottom of the coherent band. For small momenta $q \to 0$ we find the vertex $M_{\mu\nu}(\mathbf{k},\mathbf{q}) \sim q$ in the spin-fermion model, and the magnon dispersion $\omega(\mathbf{q}) \sim q$. Thus we can assume the same scaling law as in the t-J model, namely

$$a_{\mathbf{k}}(L) = a_{\mathbf{k}}(\infty) + \frac{c}{L}, \tag{3.6}$$

with L being the linear cluster dimension. The numerical data for 2D clusters with different number of sites $N = L \times L$ are presented in Fig. 10. The spin polarons are extended and therefore the smallest cluster used is 22×22; for smaller clusters the polarons do not fit to the cluster size with the present value of J, and the results are unreliable. We have found that the above simple scaling law fits quite well to our numerical data, leading to finite spectral weight of $a_{\mathbf{k}}(\infty) = 0.23$ in the thermodynamic limit for $J = 0.15$ eV. Moreover, the data show a stronger decrease in $a_{\mathbf{k}}$ with increasing

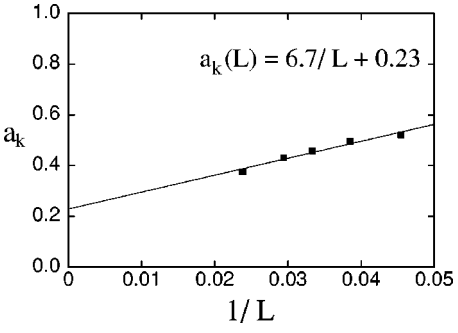

FIG. 10. Finite-size scaling of the spectral weight of the QP at $\mathbf{k} = (\pi/2, \pi/2)$ for realistic CuO_2 parameters with $\Delta_\sigma = \Delta_\pi = 5.0$ eV. The calculations were performed for systems of size $N = L \times L$ with $L = 22$, 26, 30, 34, and 42.

L by a factor larger by one order of magnitude ($c = 6.7$) than that reported for the t-J model with the corresponding parameters, where the slope was given by $c' = 0.386$ (see Fig. 16 in Ref. 13).

IV. CONCLUSIONS

We have presented a method to study the dynamics of a single oxygen hole in the Heisenberg antiferromagnet produced by copper spins in CuO_2 planes using the SCBA method. Calculating the many-body Reiter's wave function[23] we presented a systematic way to determine various spin-correlation functions and the shape of spin polaron as a function of covalency within CuO_2 planes, determined by the ratio t_{pd}/Δ_σ. We have shown that the Reiter's wave function is characterized in the present situation by rather fast convergence and only few magnon states suffice to reproduce the properties of the system, except for the regime of small $J \to 0$.

The considered spin-fermion model (2.1) includes the p_π oxygen orbitals, and we have shown by the present calculations that these orbitals are important for getting a realistic description of the spectral properties at energies far from the Fermi level. Although the QP states are quite similar when the p_π orbitals are neglected, their spectral weight increases by adding this additional channel to build the bound states. Although our main goal here was not to reproduce the experimental results, without any fitting of parameters we obtained the QP dispersion for $\Delta_\sigma = 4.5$ eV which agrees quite well with that reported for $Sr_2CuO_2Cl_2$ by Pothuizen *et al.*[3]

In spite of certain similarities, the spin polarons are qualitatively different from those reported earlier for the t-J model.[24,25] First of all, the spin polarons are more extended than in the t-J model. We believe that this follows from the oxygen hopping which diffuses the compensation cloud around the moving hole. Second, the spectral function depends strongly on the CT energy, with better QP's at large values of Δ. The QP weight increases with increasing Δ, and for $\Delta_\sigma = 5$–6 eV we found the QP states with the spectral weights of about 0.4–0.5 (see Table I), and the distribution of magnons showing the dipolarlike shape. A similar shape of the spin polaron was found for the t-J model,[24,25] although with stronger spin fluctuations around the hole. In contrast, in the region of decreasing Δ_σ with the increased Kondo coupling J_K the mechanism of the formation of ZR bound states changes, and they propagate mainly by the exchange of collective excitations (in the strong-coupling regime). Especially in this regime the polarons propagate differently, and their shape is different from that found at larger values of Δ.

In our model the electron-phonon interactions were neglected. As shown by Ramšak *et al.*[43] for the t-J model calculations (with couplings of holes to spin waves and an Einstein phonon mode included) the slow motion of the polaron for large J/t enhances the effect of the lattice distortion, resulting in a QP mass enhancement. This indicates that in order to make a more quantitative comparison with the experiment this interaction leading to some decrease of the QP bandwidth should also be taken into account.

Finally, unlike in the t-J model, the QP states do not exist in the whole range of $\mathbf{k}$, but only in certain parts of the BZ.

This was best illustrated by the comparison of the calculated spectral functions with those measured in the ARPES experiments.[3] Furthermore, in the regime of $\Delta_\sigma = 3-4$ eV the coherent bound states form only very close to the $(\pi/2,\pi/2)$ point, and their spectral weight is much smaller than that reported in the SCBA, or in the exact diagonalization calculations for the t-J model (see Table I). Therefore the low-energy sector of the spectra and the correlation functions in this regime do not resemble those obtained by Ramšak and Horsch in the SCBA calculations for the t-J model.[24,25]

ACKNOWLEDGMENTS

It is a pleasure to thank P. Horsch for stimulating discussions. One of us (J.B.) acknowledges the support of the MPI für Physik komplexer Systeme, Dresden, where the numerical part of this work was performed. We acknowledge the financial support by the Committee of Scientific Research (KBN) of Poland, Project No. 2 P03B 175 14.

APPENDIX A: THE HOLE HOPPING HAMILTONIAN

Below we specify the form of an 8×8 matrix $[H_h(\mathbf{k})]_{\mu\mu'}$ which describes the hole oxygen states in an antiferromagnet. Using these basis states for the momenta $\mathbf{k}$ and $\mathbf{k}+\mathbf{Q}$, this matrix may be represented as follows:

$$[H_h](\mathbf{k}) = \begin{pmatrix} [\hat{H}](\mathbf{k}) & [\hat{G}](\mathbf{k}) \\ [\hat{G}](\mathbf{k}) & [\hat{H}](\mathbf{k}+\mathbf{Q}) \end{pmatrix}, \tag{A1}$$

where $[\hat{H}](\mathbf{k})$ and $[\hat{G}](\mathbf{k})$ are 4×4 matrices constructed by the 2×2 blocks corresponding to the states σ and π, respectively. The $[\hat{H}](\mathbf{k})$ and $[\hat{G}](\mathbf{k})$ 4×4 matrices refer to the $2p_\sigma$ and $2p_\pi$ states and have the following block form:

$$[\hat{H}](\mathbf{k}) = \begin{pmatrix} [H^0_\sigma](\mathbf{k}) + [H^J_\sigma](\mathbf{k}) & [H^0_{\sigma\pi}](\mathbf{k}) \\ [H^0_{\sigma\pi}](\mathbf{k}) & [H^0_\pi](\mathbf{k}) \end{pmatrix}, \tag{A2}$$

$$[\hat{G}](\mathbf{k}) = \begin{pmatrix} \lambda_s[H^{AF}_\sigma](\mathbf{k}) & 0 \\ 0 & 0 \end{pmatrix}, \tag{A3}$$

where $[H^0_{\sigma(\pi)}]$, $[H^0_{\sigma\pi}]$, $[H^J_\sigma]$, and $[H^{AF}_\sigma]$ represent the following 2×2 matrices:

$$[H^0_{\sigma(\pi)}](\mathbf{k}) = \begin{pmatrix} \Delta_{\sigma(\pi)} & 4t_{pp}\sin\frac{k_x}{2}\sin\frac{k_y}{2} \\ 4t_{pp}\sin\frac{k_x}{2}\sin\frac{k_y}{2} & \Delta_{\sigma(\pi)} \end{pmatrix}, \tag{A4}$$

$$[H^0_{\sigma\pi}](\mathbf{k}) = -4t'_{pp}\cos\frac{k_x}{2}\cos\frac{k_y}{2}\begin{pmatrix} 0 & 1 \\ 1 & 0 \end{pmatrix}, \tag{A5}$$

$$[H^J_\sigma](\mathbf{k}) = 4T_K\begin{pmatrix} \sin^2\frac{k_x}{2} & -\sin\frac{k_x}{2}\sin\frac{k_y}{2} \\ -\sin\frac{k_x}{2}\sin\frac{k_y}{2} & \sin^2\frac{k_y}{2} \end{pmatrix}, \tag{A6}$$

$$[H^{AF}_\sigma](\mathbf{k}) = J_K\begin{pmatrix} -\sin k_x & 2\cos\frac{k_x}{2}\sin\frac{k_y}{2} \\ 2\sin\frac{k_x}{2}\cos\frac{k_y}{2} & -\sin k_y \end{pmatrix}. \tag{A7}$$

Here we adopt the units with the Cu-Cu distance (the unit-cell length) $a=1$, and we take the reference energy of a hole on $3d_{x^2-y^2}$ orbital $\varepsilon_d = 0$. Δ_π is the CT gap for the holes occupying p_π orbitals, while t_{pp} and t'_{pp} are direct oxygen-oxygen hopping elements between the pairs of $2p_{\sigma(\pi)}$-$2p_{\sigma(\pi)}$ and $2p_{\sigma(\pi)}$-$2p_{\pi(\sigma)}$ neighboring orbitals, respectively.

APPENDIX B: NORMALIZATION OF THE WAVE FUNCTION

In this appendix we present the analytical expression for the norm, $\mathcal{N}^{(n)}_{\mathbf{k},i} = \langle \Psi^{(n)}_{\mathbf{k},i} | \Psi^{(n)}_{\mathbf{k},i} \rangle$, of the wave function $|\Psi^{(n)}_{\mathbf{k},i}\rangle$, given by Eq. (2.20), together with the explicit form of the diagrams shown in Fig. 5. The Green's function is always evaluated below the lowest pole and only its real part is nonzero. In the present model with several oxygen bands one finds the following complex form of the norm:

$$\begin{aligned}\mathcal{N}^{(n)}_{\mathbf{k},i} = W^{\mathrm{QP}}_{\mathbf{k},i}\Bigg[& 1 + N^{-1}\sum_{\mathbf{q}_1,j} M^2_{ij}(\mathbf{k},\mathbf{q}_1)G^2_j(\mathbf{k}_1,\omega_1) \\ & + N^{-2}\sum_{\mathbf{q}_1,\mathbf{q}_2,j,i_1,i'_1} M_{ii_1}(\mathbf{k},\mathbf{q}_1)M_{i'_1 i}(\mathbf{k},\mathbf{q}_1)G_{i_1}(\mathbf{k}_1,\omega_1)G_{i'_1}(\mathbf{k}_1,\omega_1)M_{i_1 j}(\mathbf{k}_1,\mathbf{q}_2)M_{j i'_1}(\mathbf{k}_1,\mathbf{q}_2)G^2_j(\mathbf{k}_2,\omega_2) + \cdots \\ & + N^{-n}\sum_{\mathbf{q}_1\cdots\mathbf{q}_n,j,i_1\cdots i_{n-1},i'_1\cdots i'_{n-1}} M_{ii_1}(\mathbf{k},\mathbf{q}_1)M_{i'_1 i}(\mathbf{k},\mathbf{q}_1)G_{i_1}(\mathbf{k}_1,\omega_1)G_{i'_1}(\mathbf{k}_1,\omega_1)M_{i_1 i_2}(\mathbf{k}_1,\mathbf{q}_2)M_{i'_2 i'_1}(\mathbf{k}_1,\mathbf{q}_2) \\ & \times G_{i_2}(\mathbf{k}_2,\omega_2)G_{i'_2}(\mathbf{k}_2,\omega_2)\times\cdots\times M_{i_{n-2}i_{n-1}}(\mathbf{k}_{n-2},\mathbf{q}_{n-1})M_{i'_{n-1}i'_{n-2}}(\mathbf{k}_{n-2},\mathbf{q}_{n-1})G_{i_{n-1}}(\mathbf{k}_{n-1},\omega_{n-1}) \\ & \times G_{i'_{n-1}}(\mathbf{k}_{n-1},\omega_{n-1})M_{i_{n-1}j}(\mathbf{k}_{n-1},\mathbf{q}_n)M_{j i'_{n-1}}(\mathbf{k}_{n-1},\mathbf{q_n})G^2_j(\mathbf{k}_n,\omega_n)\Bigg]|0\rangle. \end{aligned} \tag{B1}$$

Next, we provide an explicit form of the diagrams of Fig. 5. After straightforward calculations one finds the following

contributions to the spin deviations around the hole from the diagrams 5(a)–(e), where the contributions (b) and (e) are evaluated together with the corresponding H.c. terms:

$$N_{\mathbf{R}}^{i_0(a)} = W_{\mathbf{k},i_0}^{\mathrm{QP}} \frac{1}{N} \sum_{\mathbf{q}_1,\mathbf{q}_1'} V_1(\mathbf{q}_1,\mathbf{q}_1') \sum_{i_1} M_{i_0 i_1}(\mathbf{k},\mathbf{q}_1) M_{i_0 i_1}(\mathbf{k},\mathbf{q}_1') G_{i_1}(\mathbf{k}_1,\omega_1) G_{i_1}(\mathbf{k}_1',\omega_1'), \tag{B2}$$

$$N_{\mathbf{R}}^{i_0(b)} = W_{\mathbf{k},i_0}^{\mathrm{QP}} \frac{1}{N} \sum_{\mathbf{q}_1,\mathbf{q}_2} V_1(\mathbf{q}_1,\mathbf{q}_2) \sum_{i_1} M_{i_0 i_1}(\mathbf{k},\mathbf{q}_1) M_{i_0 i_1}(\mathbf{k}_1,\mathbf{q}_2) G_{i_1}(\mathbf{k}_1,\omega_1) G_{i_0}(\mathbf{k}_2,\omega_2), \tag{B3}$$

$$N_{\mathbf{R}}^{i_0(c)} = W_{\mathbf{k},i_0}^{\mathrm{QP}} \frac{1}{N} \sum_{\mathbf{q}_1,\mathbf{q}_2,\mathbf{q}_2',i_2} V_1(\mathbf{q}_2,\mathbf{q}_2') \left[\sum_{i_1} M_{i_0 i_1}(\mathbf{k},\mathbf{q}_1) M_{i_1 i_2}(\mathbf{k}_1,\mathbf{q}_2) G_{i_1}(\mathbf{k}_1,\omega_1) G_{i_2}(\mathbf{k}_2,\omega_2) \right]$$
$$\times \left[\sum_{i_3} M_{i_0 i_3}(\mathbf{k},\mathbf{q}_1) M_{i_3 i_2}(\mathbf{k}_1,\mathbf{q}_2') G_{i_3}(\mathbf{k}_1,\omega_1) G_{i_2}(\mathbf{k}_2',\omega_2') \right], \tag{B4}$$

$$N_{\mathbf{R}}^{i_0(d)} = W_{\mathbf{k},i_0}^{\mathrm{QP}} \frac{1}{N} \sum_{\mathbf{q}_1,\mathbf{q}_1',\mathbf{q}_2,i_2} V_1(\mathbf{q}_1,\mathbf{q}_1') \left[\sum_{i_1} M_{i_0 i_1}(\mathbf{k},\mathbf{q}_1) M_{i_1 i_2}(\mathbf{k}_1,\mathbf{q}_2) G_{i_1}(\mathbf{k}_1,\omega_1) G_{i_2}(\mathbf{k}_2,\omega_2) \right]$$
$$\times \left[\sum_{i_3} M_{i_0 i_3}(\mathbf{k},\mathbf{q}_1') M_{i_3 i_2}(\mathbf{k}_1',\mathbf{q}_2) G_{i_3}(\mathbf{k}_1',\omega_1') G_{i_2}(\mathbf{k}_2',\omega_2') \right], \tag{B5}$$

$$N_{\mathbf{R}}^{i_0(e)} = W_{\mathbf{k},i_0}^{\mathrm{QP}} \frac{1}{N} \sum_{\mathbf{q}_2,\mathbf{q}_3} V_2(\mathbf{q}_2,\mathbf{q}_3) \sum_{\mathbf{q}_1,i_2} G_{i_2}(\mathbf{k}_2,\omega_2) \left[\sum_{i_1} M_{i_0 i_1}(\mathbf{k},\mathbf{q}_1) M_{i_1 i_2}(\mathbf{k}_2,\mathbf{q}_3) G_{i_1}(\mathbf{k}_1,\omega_1) G_{i_1}(\mathbf{k}_3,\omega_3) \right]$$
$$\times \left[\sum_{i_3} M_{i_0 i_3}(\mathbf{k},\mathbf{q}_1) M_{i_3 i_2}(\mathbf{k}_1,\mathbf{q}_2) G_{i_3}(\mathbf{k}_1,\omega_1) \right]. \tag{B6}$$

The lowest-order diagrams (a) and (b) are very easy to evaluate. The following two contributions (c) and (d) can be rewritten in the form with independent summations over $\mathbf{q}_1$, $\mathbf{q}_1'$ and $\mathbf{q}_2$, $\mathbf{q}_2'$ momenta, respectively, making their numerical evaluation technically much faster. Unfortunately, the diagram (e) does not obey this symmetry and requires more time for the numerical calculation of the correlation functions.

*Permanent address.

[1] J. G. Bednorz and K. A. Müller, Z. Phys. B: Condens. Matter **64**, 189 (1986).

[2] B. O. Wells, Z. X. Shen, A. Matsuura, D. M. King, M. A. Kastner, M. Greven, and R. J. Birgeneau, Phys. Rev. Lett. **74**, 964 (1995).

[3] J. J. M. Pothuizen, R. Eder, N. T. Hien, M. Matoba, A. A. Menovsky, and G. A. Sawatzky, Phys. Rev. Lett. **78**, 717 (1997); J. J. M. Pothuizen, Ph.D. thesis, University of Groningen, 1998.

[4] F. C. Zhang and T. M. Rice, Phys. Rev. B **37**, 3759 (1988).

[5] L. H. Tjeng, B. Sinkovic, N. B. Brookes, J. B. Goedkoop, R. Hesper, E. Pellegrin, F. M. F. de Groot, S. Altieri, S. L. Hulbert, E. Shekel, and G. A . Sawatzky, Phys. Rev. Lett. **78**, 1126 (1997).

[6] A. Nazarenko, K. J. E. Vos, S. Haas, E. Dagotto, and R. J. Gooding, Phys. Rev. B **51**, 8676 (1995).

[7] J. Bała, A. M. Oleś, and J. Zaanen, Phys. Rev. B **52**, 4597 (1995).

[8] B. Kyung and R. A. Ferrell, Phys. Rev. B **54**, 10 125 (1996); T. Xiang and J. M. Wheatley, *ibid.* **54**, 12 653 (1996); V. I. Belinicher, A. L. Chernyshev, and V. A. Shubin, *ibid.* **54**, 14 914 (1996).

[9] A. Ramšak and P. Prelovšek, Phys. Rev. B **42**, 10 415 (1990).

[10] V. V. Kabanov and A. Vagov, Phys. Rev. B **47**, 12 134 (1993).

[11] O. A. Starykh, O. F. de Alcantara Bomfim, and G. F. Reiter, Phys. Rev. B **52**, 12 534 (1995); H. Eskes and R. Eder, *ibid.* **54**, 14 226 (1996); F. Lemma and A. A. Aligia, *ibid.* **55**, 14 092 (1997).

[12] J. Bała, A. M. Oleś, and J. Zaanen, Phys. Rev. B **54**, 10 161 (1996).

[13] G. Martínez and P. Horsch, Phys. Rev. B **44**, 317 (1994).

[14] E. Dagotto, Rev. Mod. Phys. **66**, 763 (1994).

[15] J. H. Jefferson, H. Eskes, and L. F. Feiner, Phys. Rev. B **45**, 7959 (1992); L. F. Feiner, J. H. Jefferson, and R. Raimondi, *ibid.* **53**, 8751 (1996).

[16] O. K. Andersen, A. I. Liechtenstein, O. Jepsen, and F. Paulsen, J. Phys. Chem. Solids **56**, 1573 (1995).

[17] Z. X. Shen and D. S. Dessau, Phys. Rep. **253**, 1 (1995).

[18] J. Bała and A. M. Oleś, Phys. Rev. B **58**, 9408 (1998).

[19] S. Schmitt-Rink, C. M. Varma, and A. E. Ruckenstein, Phys. Rev. Lett. **60**, 2793 (1989).

[20] C. L. Kane, P. A. Lee, and N. Read, Phys. Rev. B **39**, 6880 (1989).

[21] F. Marsiglio, A. E. Ruckenstein, S. Schmitt-Rink, and C. M. Varma, Phys. Rev. B **43**, 10 882 (1991).

[22] J. Zaanen, A. M. Oleś, and P. Horsch, Phys. Rev. B **46**, 5798 (1992); J. Bała, A. M. Oleś, and J. Zaanen, Phys. Rev. Lett. **72**, 2600 (1994).

[23] G. F. Reiter, Phys. Rev. B **49**, 1536 (1994).

[24] A. Ramšak and P. Horsch, Phys. Rev. B **48**, 10 559 (1993).

[25] A. Ramšak and P. Horsch, Phys. Rev. B **57**, 4308 (1998).

[26] V. Elser, D. A. Huse, B. I. Shraiman, and E. D. Siggia, Phys. Rev. B **41**, 6715 (1990).

[27] J. Inoue and S. Maekawa, J. Phys. Soc. Jpn. **59**, 3467 (1990).

[28] J. Bonča, P. Prelovšek, and I. Sega, Phys. Rev. B **39**, 7074 (1989).
[29] P. W. Anderson, Phys. Rev. Lett. **64**, 1839 (1990).
[30] D. N. Sheng, Y. C. Chen, and Z. Y. Weng, Phys. Rev. Lett. **77**, 5102 (1996); Z. Y. Weng, D. N. Sheng, Y. C. Chen, and C. S. Ting, Phys. Rev. B **55**, 3894 (1997).
[31] K. J. von Szczepanski, P. Horsch, W. Stephan, and M. Ziegler, Phys. Rev. B **41**, 2017 (1990).
[32] C. M. Varma, S. Schmitt-Rink, and E. Abrahams, Solid State Commun. **62**, 681 (1987); V. J. Emery, Phys. Rev. Lett. **58**, 2794 (1987).
[33] J. Zaanen and A. M. Oleś, Phys. Rev. B **37**, 9423 (1988).
[34] Z. Liu and E. Manousakis, Phys. Rev. B **45**, 2425 (1992).
[35] We have chosen the somewhat stronger Coulomb repulsion than the value determined from the LDA calculations (Ref. 37) to balance the strength of the Kondo coupling which is somewhat overestimated as it follows from the second-order perturbation expansion.
[36] M. S. Hybertsen, M. Schlüter, and N. E. Christensen, Phys. Rev. B **39**, 9028 (1989); A. K. McMahan, J. F. Annett, and R. M. Martin, *ibid.* **42**, 6268 (1990).
[37] J. B. Grant and A. K. McMahan, Phys. Rev. B **46**, 8440 (1992).
[38] H. Eskes and J. H. Jefferson, Phys. Rev. B **48**, 9788 (1993).
[39] H. Eskes, G. A. Sawatzky, and L. F. Feiner, Physica C **160**, 424 (1989); J. F. Annett, R. M. Martin, A. K. McMahan, and S. Satpathy, Phys. Rev. B **40**, 2620 (1989); T. Tohyama and S. Maekawa, *ibid.* **49**, 3596 (1994).
[40] M. A. Kastner, R. J. Birgenau, G. Shirane, and Y. Endoh, Rev. Mod. Phys. **70**, 897 (1998).
[41] L. P. Gorkov and P. Kumar, Philos. Mag. B **75**, 319 (1997).
[42] E. Dagotto and J. R. Schrieffer, Phys. Rev. B **43**, 8705 (1991).
[43] A. Ramšak, P. Horsch, and P. Fulde, Phys. Rev. B **46**, 14 305 (1992).